



OPEN

Enhancement of mechanical and corrosion resistance properties of electrodeposited Ni–P–TiC composite coatings

Osama Fayyaz^{1,2}, Adnan Khan¹, R. A. Shakoor^{1✉}, Anwarul Hasan², Moinuddin M. Yusuf¹, M. F. Montemor³, Shahid Rasul⁴, Kashif Khan⁵, M. R. I. Faruque⁶ & Paul C. Okonkwo⁷

In the present study, the effect of concentration of titanium carbide (TiC) particles on the structural, mechanical, and electrochemical properties of Ni–P composite coatings was investigated. Various amounts of TiC particles (0, 0.5, 1.0, 1.5, and 2.0 g L⁻¹) were co-electrodeposited in the Ni–P matrix under optimized conditions and then characterized by employing various techniques. The structural analysis of prepared coatings indicates uniform, compact, and nodular structured coatings without any noticeable defects. Vickers microhardness and nanoindentation results demonstrate the increase in the hardness with an increasing amount of TiC particles attaining its terminal value (593HV₁₀₀) at the concentration of 1.5 g L⁻¹. Further increase in the concentration of TiC particles results in a decrease in hardness, which can be ascribed to their accumulation in the Ni–P matrix. The electrochemical results indicate the improvement in corrosion protection efficiency of coatings with an increasing amount of TiC particles reaching to ~92% at 2.0 g L⁻¹, which can be ascribed to a reduction in the active area of the Ni–P matrix by the presence of inactive ceramic particles. The favorable structural, mechanical, and corrosion protection characteristics of Ni–P–TiC composite coatings suggest their potential applications in many industrial applications.

Corrosion is the gradual destruction of metal because of the chemical reaction with its environment. Corrosion has a large share in the failure of equipment and loss of production. Corrosion behaves like a slow poison for the destruction of industrial finished products, machinery, pipelines from onshore to offshore sites etc^{1,2}. Corrosion is the major challenge faced by many industries nowadays due to various failures such as fatigue stress initiation and creep failure rooting back to corrosion³. Corrosion of valves in the reverse osmosis system results in equipment failure⁴. The loss of containment in the onshore pipelines is threatened by the corrosive environment⁵. One of the various corrosion types, such as pitting, is one of the hazardous forms of corrosion in marine and offshore structures⁶. Nearly 10 to 30% of the maintenance budget is spent on corrosion control by the oil refinery plants, as deduced by Finšgar et al.⁷. Shekari et al.⁸ mentioned the report of NACE, which estimated the global cost of corrosion to be US\$2.5 trillion in 2013, which was equivalent to 3.4% of the Gross Domestic Product (GDP).

Understanding of corrosion mechanism has led to the development of various techniques to prevent and minimize corrosion damages. Surface modification techniques provide a dual benefit of corrosion prevention and improvement of the surface properties such as hardness, abrasion, wear, inertness, and erosion, avoiding replacing the bulk of material⁹. Various surface modification techniques like carburizing, nitriding, carbonitriding, flame hardening, laser hardening, chemical vapor deposition and physical vapor deposition, etc. have been reported in the literature¹⁰. Providing a barrier between the corroding environment and the base metal with a corrosion-resistant layer is termed as a coating, which is primarily applied to prevent the loss of metal. The coating of base metal with a varying thickness can be carried out in various ways¹¹. Electrodeposition coating

¹Center for Advanced Materials (CAM), Qatar University, 2713 Doha, Qatar. ²Department of Mechanical and Industrial Engineering, College of Engineering, Qatar University, 2713 Doha, Qatar. ³Departamento de Engenharia Química, Centro de Química Estrutural, Instituto Superior Técnico, Universidade de Lisboa, Av Rovisco Pais, 1049-001 Lisboa, Portugal. ⁴Department of Mechanical and Construction Engineering, Northumbria University, Newcastle, UK. ⁵School of Mechanical, Aerospace and Automotive Engineering, Coventry University, Coventry, UK. ⁶Space Science Centre, Institute of Climate Change of the Universiti Kebangsaan Malaysia (UKM), Bangi, Malaysia. ⁷Department of Mechanical and Mechatronics Engineering, College of Engineering, Dhofar University, Salalah, Oman. ✉email: shakoor@qu.edu.qa

has gained wide acceptance in academia and industries due to its cost-effectiveness, simplicity, and capability to produce expeditious results^{12,13}. It is also used in the decorative sector, and the growth of the electroplating market is forecasted to reach US\$ 21 billion by 2026¹⁴.

Ni–P coatings have found applications in numerous industries such as aerospace, electronics, and automotive due to their good wear resistance, a higher degree of hardness, lower friction coefficient, and interesting anti-corrosive resistance¹⁵. A careful selection of coating bath composition and optimization of electrodeposition parameters is vital to achieving the desired properties of Ni–P coating, leading to widening their range of applications^{16,17}. There are mainly two proposed mechanisms for the formation of Ni–P coatings over a substrate in the respective chemical bath and operating conditions, namely direct and indirect mechanisms. Among these two, the latter i. e. indirect coating mechanism is mainly supported by the majority of the researchers. More details about the mechanism of electrodeposition of Ni–P coatings on the substrates can be glanced in the review¹⁶. Ni–P coatings have the edge over other alloy coatings such as Ni–Cu, Ni–Fe, and Ni–Co and even Ni-composites for the fabrication of microsystems¹⁸. For instance, Ni–P–Co coatings are reported to have better hardness and lubricity, along with many other appealing characteristics^{19,20}. Various chemical baths consisting of sulfate, sulfamate, and methanesulfonate have been reported in the literature for obtaining Ni–P coatings²¹.

Co-deposition of reinforcing particles to enhance Ni–P coatings specific properties through composites formation is a leading trend in the academic and classical industries^{22–24}. Recently, research in the area of Ni–P composite coatings is quite common, which has led to the development of some novel composite coating systems^{9,25–33}. Although the Ni–P–X (X = TiO₂, SiO₂, ZrO₂, CeO₂ etc.) composite coatings are grabbing substantial attention^{34–37}, the effect of electrodeposited titanium carbide (TiC) has not been fully investigated in spite of its attractive properties such as high hardness, wear resistance, corrosion resistance and high stability at elevated temperature^{38,39}. The present study deals with the synthesis and characterization of Ni–P–TiC composite coatings developed through conventional electrodeposition techniques. This work is mainly focused on the electrodeposition which is completely different technique from electroless deposition. Also, the chemical bath modified and the optimized parameters for our study is completely different from the previously reported work. Moreover, our study also considers the effect of increasing the TiC particles (<200 nm) which on one hand improves the mechanical properties through matrix-reinforcement composite phenomenon and on other hand improves the corrosion resistance by blocking the active surface area. This further endorses the novelty of our present study that the effect of various TiC particles concentrations on the structural, surface, mechanical, and corrosion-resistant properties of Ni–P coatings have been deeply investigated. The results evidence an improvement in the mechanical properties and corrosion resistance supporting the use of Ni–P–TiC composite coatings for onshore and off shore pipelines⁴⁰, tool finish and machining hard surfaces⁴¹, microsystems and micro engines¹⁸, as a replacement for hard chromium coatings¹⁶, and catalytic coatings for hydrogen evolution in water electrolysis¹⁶ etc.

Material and methods

Materials. Nickel sulphate hexahydrate, nickel chloride hexahydrate, boric acid, orthophosphoric acid, and sodium hypophosphite were bought from the Sigma Aldrich, Germany. Sodium chloride and submicron-sized titanium carbide (TiC) powder with an average particle size <200 nm and purity of 99.9% were also imported from Sigma Aldrich.

Sample preparation and coatings synthesis. The electrodeposition of Ni–P and Ni–P–TiC composite coatings was carried out on the mild steel substrate. Firstly, the mild steel sheet was cut down to the 32 mm square sheets through sheet metal operation. The mild steel samples were then polished to obtain a mirror-like surface with SiC abrasive papers of grit size 120, 220, 320, 500, 800, 1000, and 1200. The substrates were washed with soap and water before moving to the next abrasive paper. After grinding, the substrates were sonicated in the acetone for half an hour. One side of the substrates was covered with insulating tape to avoid electrodeposition on both sides of the substrates. The substrates were activated in 20% HCl solution for about 45 s, rinsed in distilled water, and finally put in the coating bath. During the electrodeposition process, the dc power supply's negative electrode was connected to the substrate forming a cathode, and the positive electrode of the power supply was connected to the nickel sheet to provide an anode. The schematic diagram of the electrodeposition experimental setup is represented in Fig. 1. The nickel sheet (anode) and the substrate (cathode) were placed parallel and face to face each other at a distance of approximately 30 mm in the coating bath. The optimized electrodeposition conditions are tabulated in Table 1. Ni–P and Ni–P–TiC composite coatings were developed at 65 °C ± 2. The time of the coatings is half an hour from the start of the power supply. The coating bath was agitated at 300 ± 5 rpm for 60 min before initiating the electrodeposition process to avoid settling down of the TiC particles. The coating bath was kept agitated during the entire coating process at 300 rpm for uniform distribution of reinforcing particles into the Ni–P matrix.

Sample characterization. The thickness of the synthesized Ni–P and Ni–P–TiC composite coatings was determined by thickness gauge (model BDYSTD-E, USA). Structural characterization of the synthesized coatings was carried out employing X-ray diffractometer (PANalytical, Empyrean, UK) fitted with Cu K α radiations with the scanning step of 0.02° in the range of 2 θ from 10° to 90°. The field emission scanning electron microscope (FE-SEM-Nova Nano-450, Netherlands), atomic force microscopy (AFM-USA) and high-resolution transmission electron microscope (HR-TEM FEI : TECNAI G2 FEG 200 kV) were used to perform the morphological study. The composition of the prepared coatings was also determined by X-ray photoelectron spectroscopy—XPS (Kratos Analytical Ltd, UK) using a monochromatic Al-K α X-Ray source. The hardness of the prepared coatings was tested with Vickers microhardness tester (FM-ARS9000, USA). The measurement of the

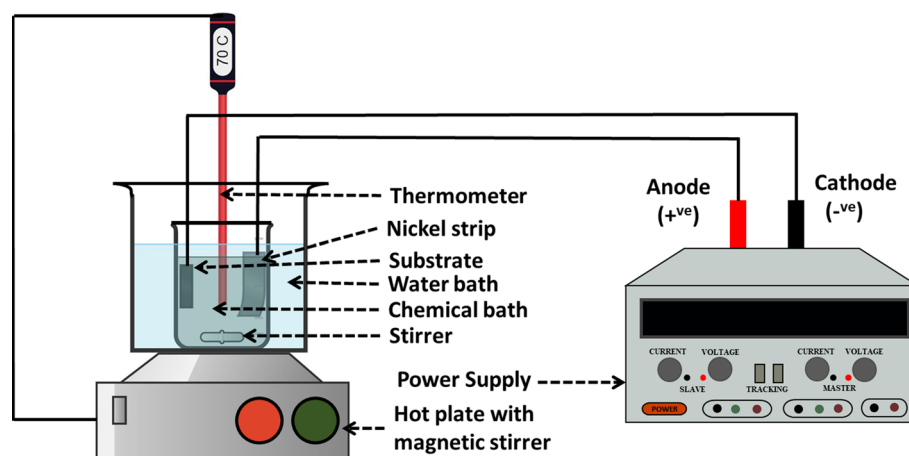


Figure 1. Schematic diagram of the electrodeposition process to develop Ni–P–TiC composite coatings.

Chemical bath and operating conditions	Bath Ni–P/TiC
Nickel Sulfate hexahydrate	250 g L ⁻¹
Nickel Chloride hexahydrate	15 g L ⁻¹
Boric acid	30 g L ⁻¹
Sodium Chloride	15 g L ⁻¹
Phosphoric acid	6 g L ⁻¹
Sodium hypophosphite	20 g L ⁻¹
TiC particles concentration	0, 0.5 g L ⁻¹ , 1 g L ⁻¹ , 1.5 g L ⁻¹ and 2 g L ⁻¹
pH	2.0 ± 0.2
Bath temperature	65 ± 2 °C
Deposition time	30 min
Current density	50 mA/cm ²
Bath agitation	300 rpm

Table 1. Optimized bath composition and parameters for co-electrodeposition of Ni–P–TiC composite coatings.

microhardness was carried out at 100 gf with the dwell time of 10 s on the surface of the coatings. The nanoindentation measurements were performed employing AFM device MFP-3D Asylum research (USA) equipped with silicon probe (Al reflex coated Veeco model-OLTESPA, Olympus; spring constant: 2 Nm⁻¹, resonant frequency: 70 kHz). All measurements were carried out under ambient conditions using standard topography A.C. air (tapping mode in the air). The indentation was performed with Berkovich diamond indenter tip with a maximum 1mN indentation force (loading and unloading rate: 200 μN/s and dwell time at maximum load: 5 s). Oliver and Pharr's method was used to find contact penetration from the unloading curves. The electrochemical impedance spectroscopy (EIS) studies were carried out with Gamry cell in which saturated silver/silver chloride (Ag/AgCl) was used as the reference electrode, whereas graphite and prepared coated samples were employed as counter and working electrodes, respectively. EIS was measured by AC signal with 10 mV of amplitude within the frequency range of 10²–10⁻² Hz at open circuit potential. Moreover, potentiodynamic studies were carried out at ambient room temperature with a scan rate of 0.167 mV s⁻¹ after the determination of open circuit potential for more than 10 min of stabilization of complete cell. A constant surface area of 0.765 cm² of all tested samples was exposed to 3.5 wt% NaCl solution in the entire study^{33,42,43}.

Results and discussion

XRD analysis. The structural analysis of the electrodeposited Ni–P and Ni–P–TiC composite coating was carried out through XRD and the spectra of NiP and Ni–P–TiC composite coatings containing various compositions of TiC (0, 0.5, 1.0, 1.5, 2 g L⁻¹) are shown in Fig. 2. The semi-amorphous structure of the coatings can be deduced from the broad peaks in all the cases, and the broad peak located at 2θ ~ 45.5 can be assigned to the Ni (111) plane of face-centered cubic (FCC) structure. The formation of an amorphous structure can be ascribed to the lattice distortion experienced by the nickel crystal structure due to the presence of phosphorous atoms, which hinders the propagation of face-centered cubic occupancy of nickel atoms⁴⁴. The amorphous nature of the coatings has already been reported^{10,15,45} along with nanocrystalline structure as reported in the literature^{46,47}.

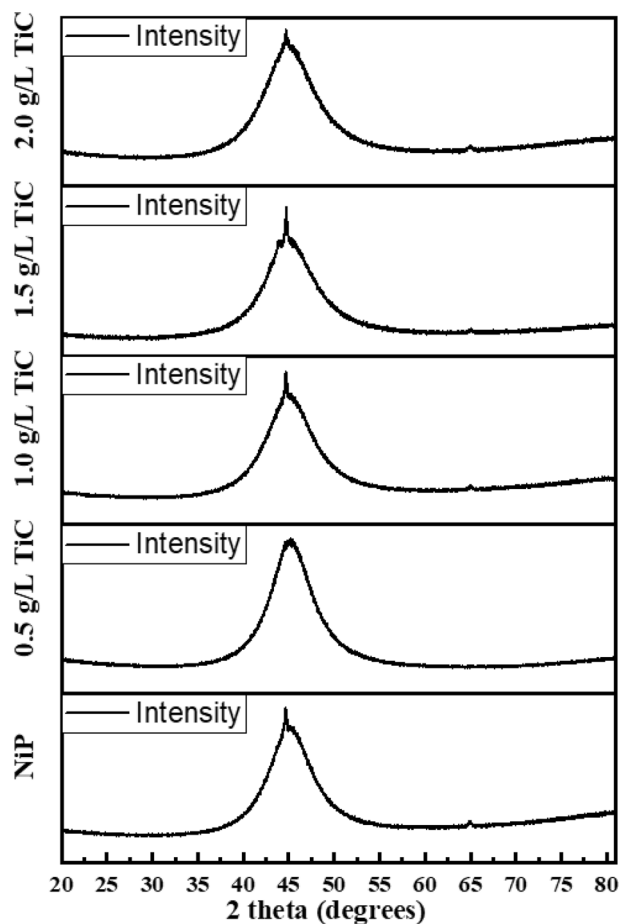


Figure 2. XRD spectra of Ni-P and Ni-P-TiC composite coatings containing various concentrations of TiC particles.

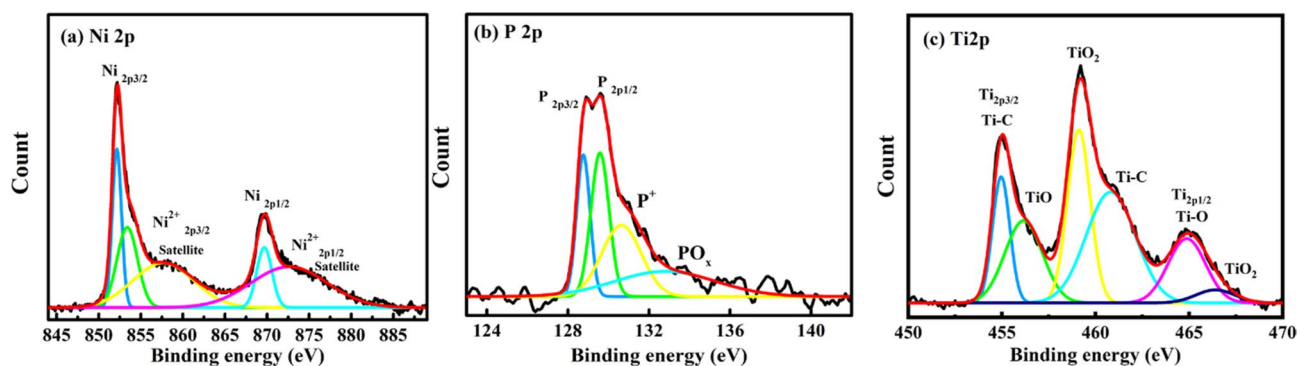


Figure 3. XPS spectra presenting the elemental composition of Ni-P/1.5 g L⁻¹ TiC composite coatings, (a) Ni2p, (b) P2p and (c) Ti2p.

The diffraction peaks of the TiC were not observed in the XRD spectra, probably due to their low contents in the Ni-P matrix. Similar results have also been reported in the literature^{29,48}.

XPS analysis. The presence of TiC in the Ni-P TiC composite coatings was confirmed using XPS analysis. To avoid any repetition, the fitted data of individual photoionizations and their corresponding chemical states only the 1.5 g L⁻¹ TiC composition is presented in Fig. 3. High energy resolution spectra of Ni2p (Fig. 3a) region contains two distinct ionizations: Ni 2p_{3/2} and Ni 2p_{1/2} at 852.2 eV and 869.9 eV assigned to Ni in the metallic state, whereas the peaks of Ni²⁺ at 853.3 eV, 857.6 eV, and 872.7 eV corresponds, respectively to the NiO and/or Ni(OH)₂ of Ni 2p_{3/2} and Ni 2p_{1/2}. The high intensity peak for nickel proves the presence of metallic nickel. The formation of Ni(OH)₂ and NiO can be linked to the presence of hydroxyl ion from the aqueous electrolytic bath

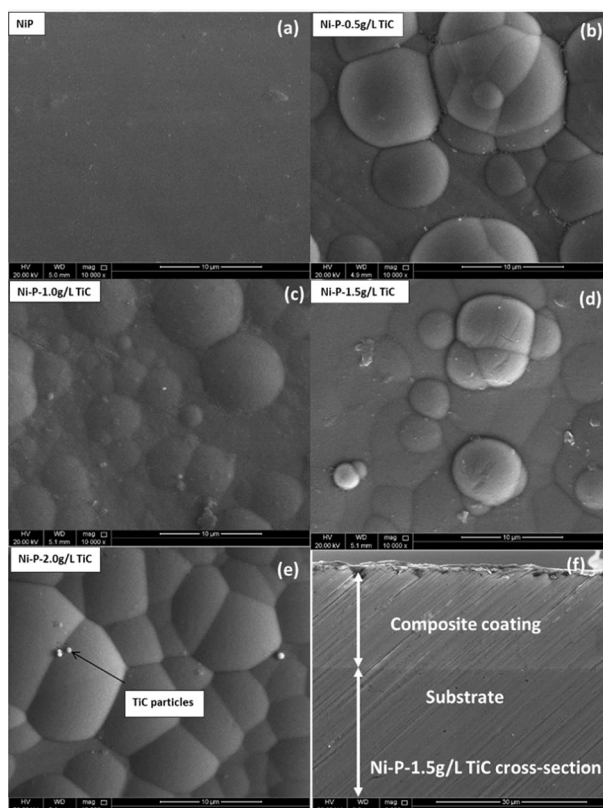


Figure 4. FE-SEM micrographs of the Ni-P (a) and Ni-P-TiC composite coating with various concentrations of TiC (b,c,d,e). A cross-sectional micrograph (f) of Ni-P-TiC composite coatings with 1.5 g L⁻¹ of TiC.

Coatings Composition	Average coating thickness
Ni-P	17 μm ± 2
Ni-P 0.5 g L ⁻¹ TiC	17 μm ± 2
Ni-P 1.0 g L ⁻¹ TiC	17.4 μm ± 2
Ni-P 1.5 g L ⁻¹ TiC	17.2 μm ± 2
Ni-P 2.0 g L ⁻¹ TiC	17.6 μm ± 2

Table 2. Average thickness of Ni-P and Ni-P-TiC composite coatings measured with thickness gauge meter.

and other surface oxidation phenomenon^{33,49}. Concerning the P2p ionization, the peaks at 128.8 and 129.5 eV can be assigned to the elemental phosphorous (P) in the bulk of electrodeposited Ni-P-TiC composite coating, respectively (Fig. 3b). It can be noticed that the peak at 130.69 eV is due to (i) elemental phosphorus hypophosphite and/or (ii) intermediate phosphorous ions (P(I) and/or P(III)) valence which are presented in the inner portion of the protective film of the Ni-P coatings. However, peaks at 132.7 eV can be due to the combination of oxides and/or hydroxides (P₂O₃ and/or P-OH) chemical states³³. The high-resolution spectra of the Ti2p spectrum were deconvoluted into three doublet peaks (Fig. 3c) of titanium carbide, based at 454.9 and 460.8 eV, titanium oxides at 456.1 and 464.8 eV and TiO₂ at 459.2 and 466.4 eV as previously reported^{50,51}.

Microstructural analysis. The morphology of the Ni-P and Ni-P/TiC composite coatings containing various concentrations of TiC particles was studied with FE-SEM as specified in Fig. 4. Ni-P coatings (Fig. 4(a)) does not show the formation of a well-defined nodular structure. A similar morphology of Ni-P coatings has been reported in the literature^{29,52}. On the other hand, FE-SEM micrographs of Ni-P-TiC composite coatings (Fig. 4b-e) show the compact, nodular morphology without any noticeable defects. The presence of TiC particles can also be observed in the FE-SEM images, especially at the 2.0 g L⁻¹ of composition in good agreement with literature^{33,53}. Figure 4f shows the cross-section of Ni-P-TiC (1.5 g L⁻¹) composite coatings. A smooth and well-adherent coating, without any apparent defects can be observed, together with an uniform interface. A uniform coating thickness of ~ 15 μm is achieved.

The coating thickness was also measured with the coating gauge meter and presented in Table 2. It can be noticed that the coating thickness under all identical conditions are similar, and there are no noticeable changes

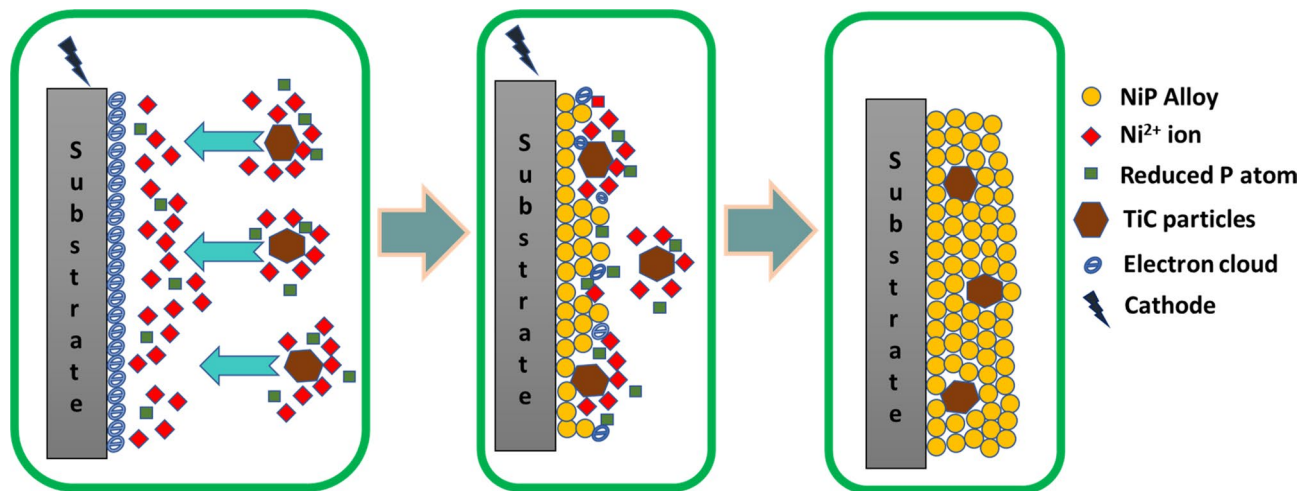


Figure 5. Schematic diagram for the co-deposition of TiC particles at the cathode (substrate) to form Ni–P–TiC composite coatings.

in the thickness. It is worthy of mentioning that the reported values are an average of five readings. A slight difference in thickness of coatings measured through FE-SEM analysis may be due to the surface preparation required for the test.

Co-deposition mechanism of various reinforcements in Ni–P matrix has been proposed by many researchers. Guglielmi⁵⁴ proposed a model containing two steps in which firstly, particles adsorb weakly on the cathode surface by Van der Waals forces and then during the second stage strong adsorption by coulombic forces. This model fails to account for particle size and hydrodynamics of the deposition. Bercot et al.⁵⁵ formulated a corrective factor to this model for accounting for magnetic stirring in their study, whereas Bahadormanesh and Dolati modified Guglielmi's model for the deposition of a high-volume percentage of the second phase and carried out a parametric study⁵⁶. Moreover, Fransaer et al. devised a trajectory model in which they presented an analysis of various forces on a spherical particle in a rotating disk electrode system⁵⁷. According to Ceils et al.⁵⁸, the electrodeposition mechanism may consist of five steps; (i), formation of an ionic cloud around the reinforcement particles, (ii) movement of reinforcement particles by forced convection towards the hydrodynamic layer of the cathode, (iii) diffusion of the particle through double layer, (iv) adsorption of the particle along with the ionic cloud at the cathode surface and (v) reduction of the ionic cloud leading to an irreversible entrapment of reinforcement particles in the metal matrix. As per the above discussion, it seems there are mainly three steps involved in the co-deposition of the reinforcement particles, such as TiC during the electrodeposition process; (i) movement of particles from bulk electrolyte to hydrodynamic boundary layer of the cathode which are governed by a combination of forced convection and electrophoresis, (ii) diffusion and adsorption of particles at the cathode due to Van der Waal forces, and (iii) permanent incorporation of particles due to the reduction of ionic cloud around the reinforced particle. This three-step phenomenon can be described in the schematic diagram in Fig. 5.

The co-electrodeposited of TiC in the Ni–P matrix was further evaluated with EDS analysis. The EDS analysis of Ni–P and Ni–P–TiC composite coatings containing various concentrations of TiC particles, is presented in Fig. 6a–f. The elemental mapping of Ni–P /TiC composite coatings is shown as an inset of Fig. 6. The presence of titanium (Ti), carbon, (C), Phosphorus (P), and nickel (Ni) confirm the incorporation of TiC particles into the Ni–P matrix. Table 3 shows the weight percentage of various elements in the as prepared composite coatings. As for Ni–P coating, nickel constitutes almost 89.51 wt.% and the remaining is balanced by phosphorus. Introduction and increase of the concentration of TiC powder in the chemical bath does affect the concentration of nickel in the deposit, which appreciably decreases without significant effect over the phosphorus content which remains around 10 wt.% in all the coatings. The titanium content in the deposits increases from 0.39 to 0.84 wt.% when the concentration in the chemical bath is increased from 0.5 to 2.0 g L⁻¹. However, the excessive weight percentage of carbon can be attributed to the combination of various effects such as presence of carbon in the titanium carbide compound, impurities related to environment and surface preparation for the microscopic analysis. Incorporation of TiC particles can be inferred from the titanium peaks in the EDS plot of 0.5, 1.0, 1.5, 2.0 g L⁻¹ and cross-section of 1.5 g L⁻¹ of TiC. The carbon peak in all the plots can be attributed to the steel substrate's carbon composition due to background interference as previously reported by Pouladi et al.⁵⁹. Peaks of iron are also observed in the cross-sectional EDS analysis which can be ascribed to the steel substrate. Further, corresponding EDS elemental mapping results shown as an inset of corresponding compositions depicts the clear distribution of Ni, P, and TiC particles in the Ni–P matrix.

In order to further investigate the microstructural properties of the deposit, high resolution-transmission electron microscopy analysis were carried out for the Ni–P–2.0 g L⁻¹ TiC. Figure 7 shows the TEM bright field micrographs of electrodeposited Ni–P–2.0 g L⁻¹ TiC composite coating at various magnifications. All the images clearly reveal the presence of a separate second phase of TiC particles within the Ni–P matrix. Figure 7a presents a low magnification micrograph of the composite coating. The excessive darkness is due to the thickness of the coating deposited on the copper grid for TEM analysis. Figure 7b is the enlarged image at the marked location

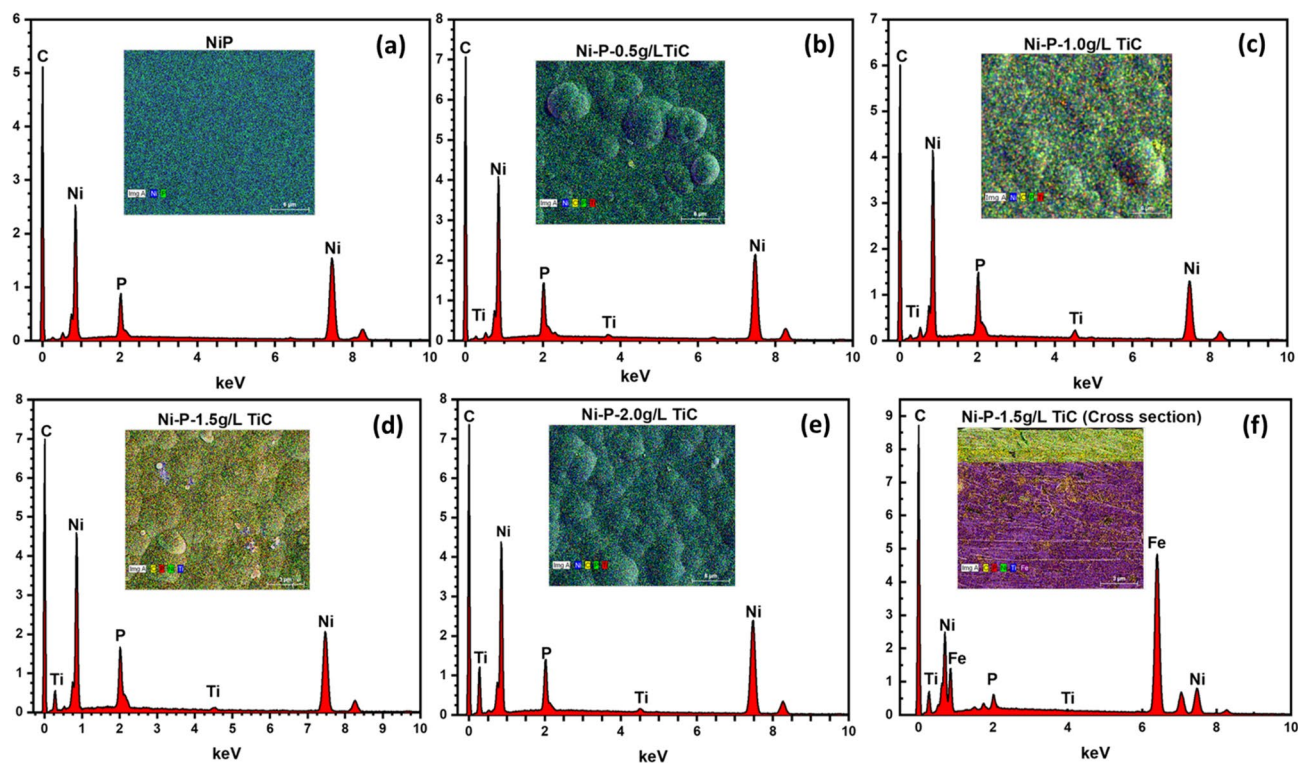


Figure 6. EDS analysis along with elemental mapping of Ni-P (a) and various compositions of Ni-P-TiC composite coatings, (b) 0.5 g L⁻¹, (c) 1.0 g L⁻¹, (d) 1.5 g L⁻¹, (e) 2.0 g L⁻¹ and (f) cross-section of 1.5 g L⁻¹ of Ni-P-TiC composite coatings.

S. no	Sample designation	Ni (wt.%)	P (wt.%)	Ti (wt.%)	C (wt.%)
1	Ni-P	89.51	10.49	–	–
2	Ni-P-0.5 g L ⁻¹ TiC	73.47	9.94	0.39	16.2
3	Ni-P-1.0 g L ⁻¹ TiC	69.74	9.82	0.64	19.8
4	Ni-P-1.5 g L ⁻¹ TiC	66.19	10.52	0.79	22.5
5	Ni-P-2.0 g L ⁻¹ TiC	66.58	9.68	0.84	22.9

Table 3. EDS quantitative analysis of Ni-P and Ni-P-TiC composite coatings.

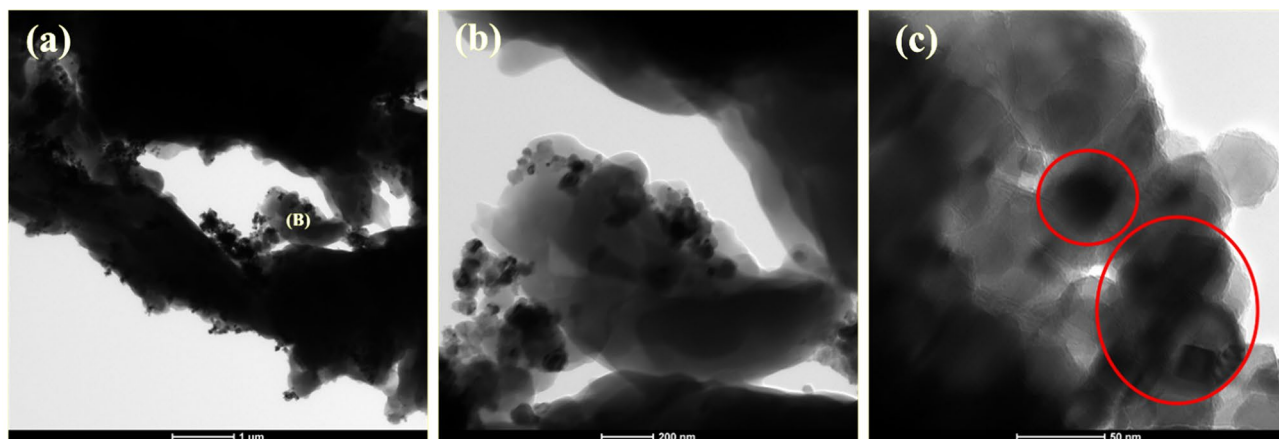


Figure 7. TEM micrographs of Ni-P-2.0 g L⁻¹ TiC at various magnification of (a) high magnification (b) magnified portion marked (B) in (a) and (c) showing an interface of the Ni-P matrix and TiC reinforcement.

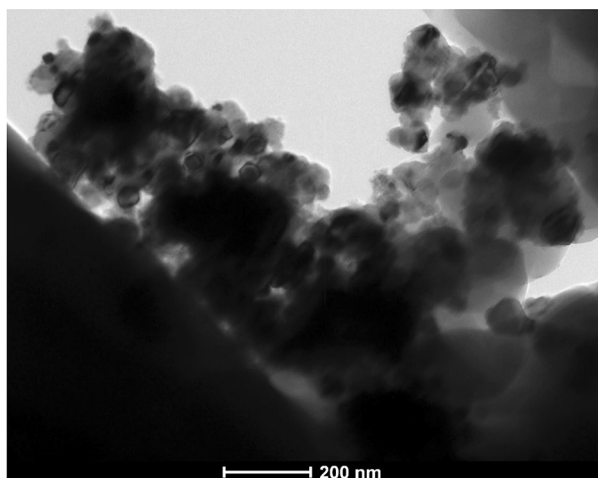


Figure 8. TEM micrograph of Ni-P-2.0 g L⁻¹ TiC presenting the agglomeration of the particles in the Ni-P matrix.

(B) in Fig. 7a presenting the amorphous structure of the composite coating with the lighter region corresponding to the nickel lattice formation as also reported by Huang et al. in their exhaustive study of microstructure in the Ni-P coating⁶⁰. An irregular dark network is observed in the Fig. 7b which is prevalent to the mid-high phosphorus content within the electrodeposited composite coatings as previously reported^{60,61}. Figure 7c is the micrograph at very high magnification presenting the cubical polygonal structure of the reinforced titanium carbide embedded in the Ni-P matrix. The matrix-reinforcement interface can be clearly distinguished as comparatively sharp contrast can be identified in the micrographs. According to literature, titanium carbide particles are reported to have regular polygonal cubical structure⁶².

FE-SEM images could not accurately provide the evidence of aggregation or agglomeration of TiC particles during the fabrication of the Ni-P-2.0 g L⁻¹ TiC composite coating. TEM analysis further confirms the agglomeration or aggregation of the cubical polygonal TiC particles, which are visible in Fig. 8 for the Ni-P-2.0 g L⁻¹ TiC. Agglomeration of the particles in composite coatings has been confirmed through TEM micrograph as reported in literature^{61,63}.

The surface topography of the electrodeposited Ni-P and Ni-P-TiC composite coatings was investigated through atomic force microscopy (AFM). Three-dimensional images of Ni-P and Ni-P/TiC composite coatings with the various compositions of TiC particles are presented in Fig. 9a–e. It is observed that the Ni-P coatings indicate a relatively smooth surface when compared with the Ni-P-TiC composite coatings. The Ni-P-TiC composite coatings' surface is composed of valleys and intrusions due presence of TiC particles into the Ni-P matrix that provides a rougher texture. The quantitative analysis of surface topography indicates that the addition of TiC particles into the Ni-P matrix has resulted in an increase in the surface roughness. The average surface roughness (Ra) increases with the increasing amount of TiC particles and the average value increased from 6.786 nm (Ni-P coatings) to 33.014 nm (Ni-P/TiC-2.0 g L⁻¹), contributing five times enhancement in the surface roughness. Moreover, Rq (root mean square value of the roughness) is also presented which shows the similar trend as the average roughness as presented in the Fig. 9. Furthermore, Rz values also displays the similar increasing trend from 18.6 nm roughness of Ni-P coating to the successive increase upto 53.8 nm, 58.5 nm, 70.2 nm and 77.6 nm for the increase in the concentration of TiC particles of 0.5 g L⁻¹, 1.0 g L⁻¹, 1.5 g L⁻¹ and 2.0 g L⁻¹ in the chemical bath. The increase in the surface roughness with an increasing amount of TiC particles can be attributed to the presence of insoluble and hard ceramic particles, which provides jerks and barriers to the free movement of the AFM cantilever tip. These findings are consistent with the previous studies^{29,33}.

Mechanical properties. *Vickers microhardness.* Vickers microhardness results of Ni-P and Ni-P-TiC composite coatings are presented in Fig. 10. As seen, Ni-P coating's hardness value is around 500HV, which increases to ~ 530 HV and ~ 550 HV on the incorporation of 0.5 g L⁻¹ and 1 g L⁻¹ of the TiC particles, respectively. The hardness value reaches its maximum value of ~ 593 HV at the composition of 1.5 g L⁻¹. The increase in the hardness is about 19%, which can be attributed to the dispersion hardening effect and improvement in the load-bearing characteristics of the matrix due to the formation of a composite structure, aligned to previously reported literature^{64,65}. After reaching to its terminal value, the microhardness decreases with further increase in TiC particles and it decreases to ~ 550 HV at 2.0 g L⁻¹. A decrease in the hardness value at 2.0 g L⁻¹ can be attributed to the excessive aggregation of the TiC particles in Ni-P matrix, which impairs the load-bearing properties of the Ni-P/TiC composite coatings. This observation is also consistent with previous reports⁶⁶.

Nanoindentation. The indentation tests of the Ni-P and Ni-P-TiC composite coatings were performed to have an insight of the mechanical response of the developed coatings. The loading/unloading indentation profiles of Ni-P and Ni-P-TiC composite coatings containing various concentrations of TiC particles are presented

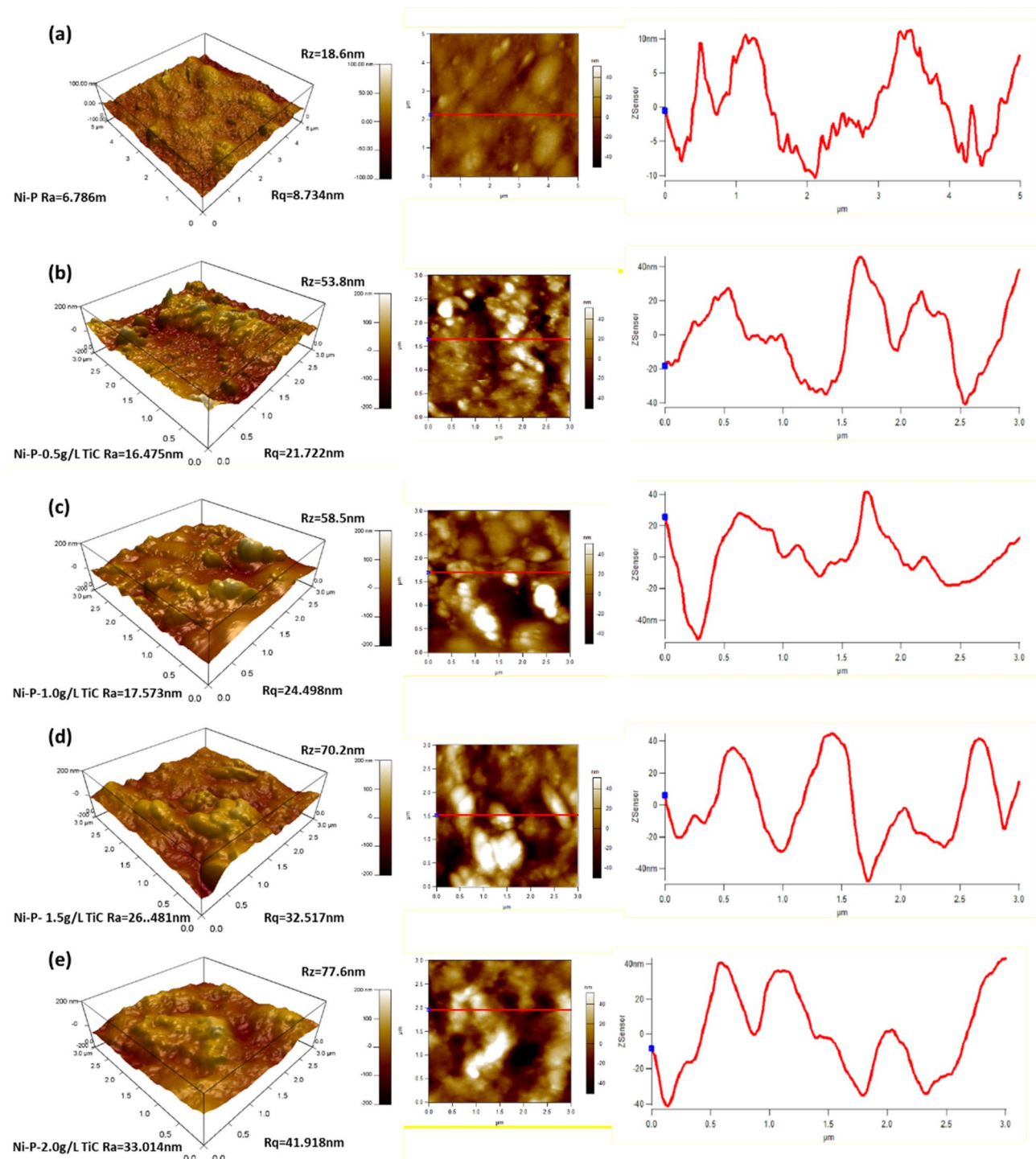


Figure 9. 3D-AFM micrograph along with their corresponding surface roughness profiles of the (a) Ni-P, Ni-P-TiC composite coatings (b) 0.5 g L⁻¹, (c) 1.0 g L⁻¹, (d) 1.5 g L⁻¹, and (e) 2.0 g L⁻¹ of TiC particles.

in Fig. 11. A gradual decrease in indentation depth with an increasing amount of TiC particles in the Ni-P matrix is evident in Fig. 11a. The Ni-P coatings demonstrate an indentation depth of ~ 50 nm, which reduces to 23.67 nm at the composition of 1.5 g L⁻¹ of TiC. The decrease in depth is due to the enhancement in the hardness of the coatings, which is directly associated with the dispersion hardening effect and improvement in the load-bearing properties, as explained previously. It can be further noticed that there is a decrease in the indentation depth of ~ 7 nm at the terminal composition (2.0 g L⁻¹ TiC). This is because of the fact that an excessive amount of reinforcement accumulates in the matrix and thus harms the mechanical properties in agreement with previous studies^{67,68}. The maximum decrease in the indentation depth is observed at 1.5 g L⁻¹ of TiC due to the uniform distribution of the reinforcing phase in the matrix without any significant agglomeration. The loading/unloading curves are uniform without any kinks, suggesting that the synthesized coatings are free of cracks

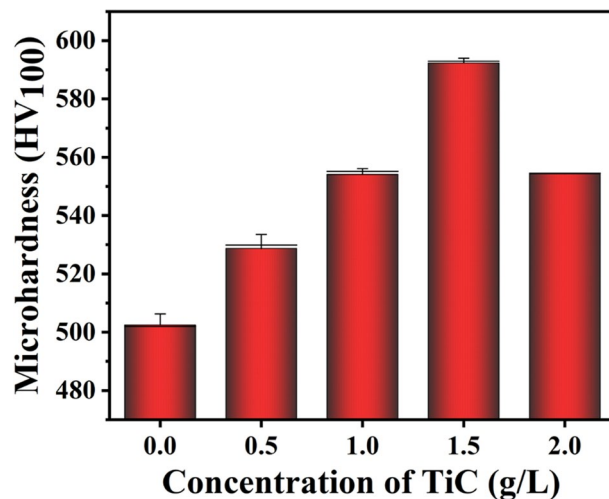


Figure 10. Vickers microhardness of Ni–P and Ni–P–TiC composite coatings containing various concentrations of TiC particles.

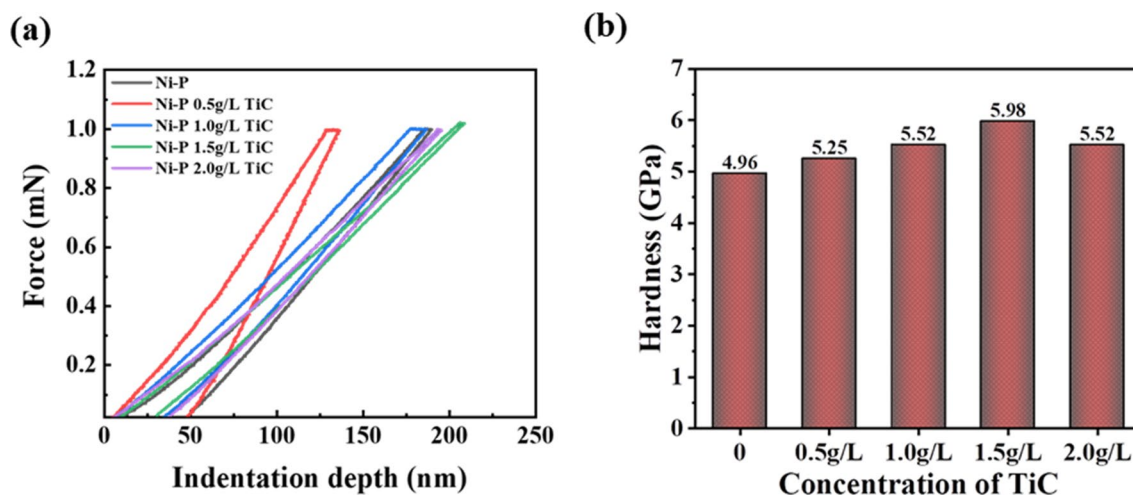


Figure 11. Nanoindentation results of Ni–P and Ni–P–TiC composite coatings containing various concentrations of TiC particles; (a) loading/unloading profiles and (b) hardness.

and pores. For more accurate comparison, a quantitative analysis of the indentation results obtained through Oliver and Pharr technique is also represented in Fig. 11b. It can be noticed that the hardness of Ni–P coatings is 4.96 GPa, which increases with increasing concentration of TiC particles in the Ni–P matrix, reaching its terminal value of 5.98 GPa at the composition of 1.5 g L⁻¹. Further increase of TiC particles concentration in the Ni–P matrix decreases hardness and it attains a value of 5.52 GPa at the TiC composition of 2.0 g L⁻¹. This result further supports the observation that incorporation of ceramic TiC increases the hardness of the NiP matrix, in good agreement with literature^{33,69}. The decrease in the hardness for 2.0 g L⁻¹ can be due to agglomeration of TiC particles in the Ni–P matrix. The nanoindentation results are in agreement with the Vickers microhardness test results.

Corrosion behavior

Electrochemical impedance spectroscopy (EIS). The corrosion resistance of the coatings was studied through electrochemical impedance spectroscopy (EIS) and potentiodynamic polarization techniques. The EIS plots (Bode plots) of the substrate (carbon steel), NiP, and NiP–TiC composite coatings containing various concentrations of TiC are presented in Fig. 12a,b. Experimental data were fitted using an equivalent circuit based on a modified Randle circuit. It is composed of two-time constants in cascade assigned to the composite coatings and metal-coating interface exposed at the bottom of conductive paths, as presented in Fig. 13a,b. The various elements in the circuit account for: R_s —electrolyte resistance, R_{po} —pore resistance, R_{ct} —polarization resistance, and constant phase elements (CPE1 and CPE2) instead of capacitors to account for surface inhomogeneity. The constant phase elements can be calculated by the following equation³³:

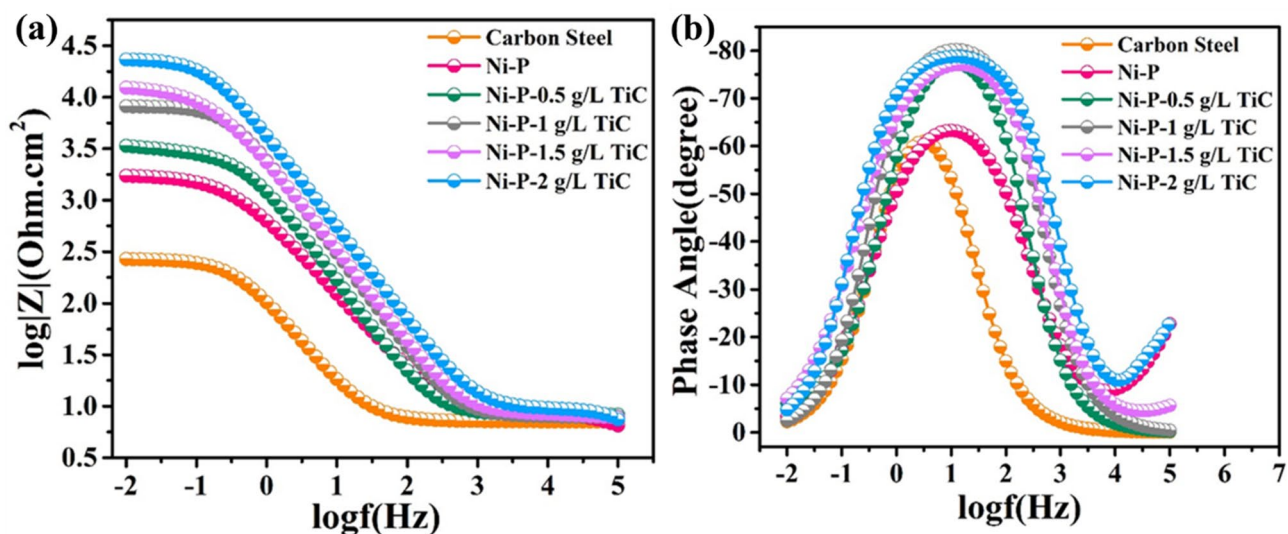


Figure 12. (a) Bode plots of the substrate, Ni-P, and Ni-P-TiC composite coatings containing the magnitude plot and (b) phase angle plot after 2 h of immersion in 3.5wt% NaCl solution.

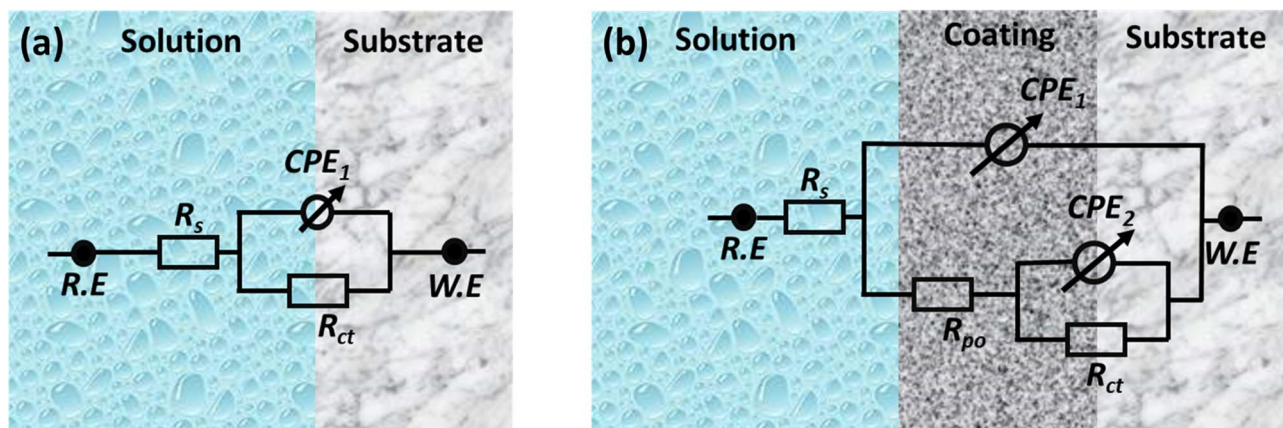


Figure 13. Equivalent electric circuit used for fitting the experimental EIS data for (a) polished carbon steel used as substrate, (b) Ni-P and Ni-P-TiC composite coatings containing different concentrations of TiC particles.

$$\frac{1}{Z_{CPE}} = Q(j\omega)^n$$

where Q is the admittance and ω is the angular frequency of the alternating signal and n is the exponent of CPE which determines the capacitance nature, i.e., when “ n ” approaches unity, the CPE approaches to pure capacitance and the element behaves like an ideal capacitor³³.

Referring to Fig. 12, the medium–high-frequency regions of the Bode plot for carbon steel evidence one time constant, while for the coated samples there is a broadening of the phase angle, suggesting two overlapped time constants—the one associated to the composite coating and another to the interfacial phenomena at the bottom of pores formed in the coating. The magnitude plot indicates that the corrosion resistance of the carbon steel sample is very low $\sim 270 \Omega \text{ cm}^2$, a value that was obtained after fitting the experimental data using the proposed equivalent circuit (Fig. 13a). Ni-P coatings show an improvement in the impedance value of one order of magnitude which can be ascribed to the formation of the hypophosphite layer due to electrochemical reactions of the salt solution with the surface of Ni-P coating^{70,71}. The inclusion of secondary phase TiC particles in the Ni-P matrix further changes the impedance response, leading to the broadening of the phase angle plot. This trend indicates, by the one hand, a more protective composite coating (shift towards higher frequencies) and, on the other hand, the presence of other processes (decreased corrosion activity) as previously reported in literature^{33,42}. The increased impedance in the composite coatings can be attributed to the reduction on the number active corrosion sites due to the occupancy of inert and corrosion-resistant TiC particles. The Ni-P-0.5 g L⁻¹ TiC showed almost doubled impedance values compared to a simple Ni-P coated sample (Fig. 12). An increase in the concentration of TiC particles from 0.5 g L⁻¹ up to 2.0 g L⁻¹ has successively increased the corrosion resistance and the maximum impedance values for Ni-P-2.0 g L⁻¹ TiC reaches 23 k $\Omega \text{ cm}^2$ showing an improvement of $\sim 92\%$ when compared to Ni-P coatings. An increase in the pore resistance can be due to

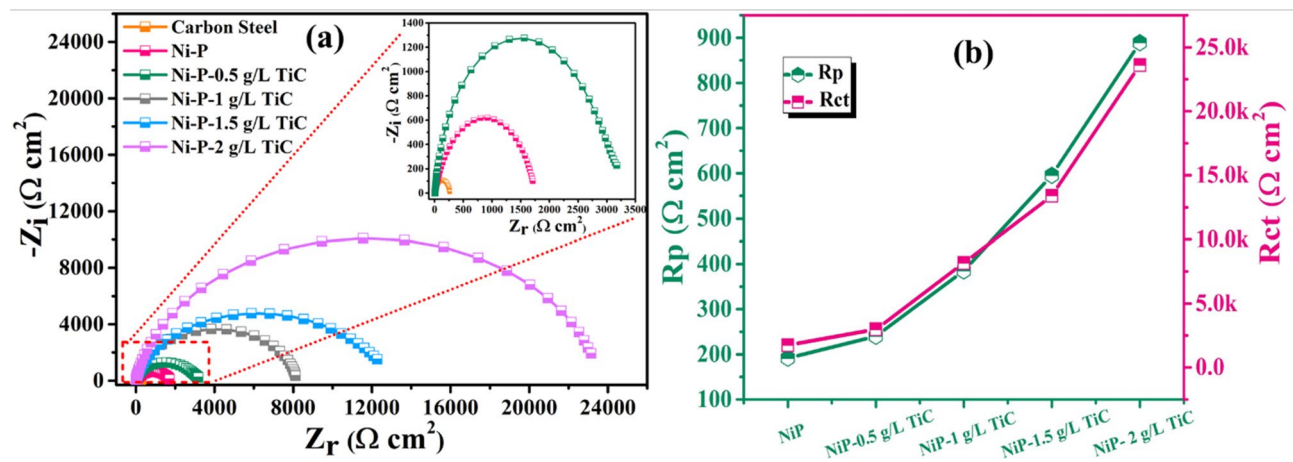


Figure 14. (a) Nyquist plots for carbon steel (substrate) and Ni–P–TiC composite coatings along with fitted resistance values vs. the concentration of TiC particles after the 2 h of immersion in 3.5wt% NaCl solution (b) evolution of R_{p0} and R_{ct} with the TiC particles concentration.

the presence of TiC particles in the pores of Ni–P matrix that decreases the number of conductive paths and increases the surface roughness as observed in AFM results⁴⁹. Improvement in the polarization resistance can be related to the successive increase in the reinforcement of TiC particles in the Ni–P matrix which hinders the electrolyte from reaching the substrate, decreasing the number of active sites and hence providing additional protection against corrosion^{33,42,49}.

Figure 14a depicts the Nyquist plots for carbon steel (substrate), Ni–P and Ni–P–TiC composite coatings containing various concentrations of TiC particles. Nyquist plots of Ni–P coatings and Ni–P–TiC composite coatings demonstrate distinct capacitive loops. The experimental plots for the coated samples were fitted using the two-time constant equivalent electric circuit described in Fig. 13b and the fitting goodness is represented in Fig. 14 in the Nyquist plots. The capacitive loop diameter evidences a successive increase, confirming the higher corrosion resistance in the presence of TiC particles. Figure 14 depicts the evolution of the pore resistance and polarization resistance over time. The incorporation of TiC particles in the Ni–P matrix increases the pore resistance in the coating and acts as a barrier by that delays electrolyte uptake. The decrease of the active surface area is responsible for the increase in the polarization resistance (R_{ct}) as shown in Fig. 14b. Moreover, increasing the concentration of TiC particles in the chemical bath leads to a decrease in the active region and, therefore, increases the corrosion resistance of the composite coatings. The enhancement in the corrosion resistance of the NiP coating in the presence of various concentrations of TiC can be enumerated by the combined effect of (i) Inert TiC particles reduce the active area in the NiP alloy (ii) TiC particles are assumed to block the pores by filling them and restricting the diffusion of the Cl^- ions towards the metal surface and (iii) double-layer capacitance reduces. These findings are consistent with the previous studies^{9,33,42,49}.

Potentiodynamic polarization analysis. The corrosion resistance of the carbon steel, Ni–P, and Ni–P–TiC composite coatings containing various concentrations of TiC particles was also studied by d.c. potentiodynamic polarization employing a scan rate of 0.167 mV s^{-1} as shown in Fig. 15. Electrochemical parameters such as corrosion potential (E_{corr}), corrosion current density (I_{corr}), anodic Tafel slope (β_a), and cathodic Tafel slope (β_c) were extrapolated from the fitted curve and tabulated in Table 4. Moreover, the corrosion protection efficiency (PE %) was calculated from the formula as reported³³.

$PE\% = 1 - \frac{i_2}{i_1}$ where i_1 is the current density of the carbon steel and i_2 is the current density of coated samples. The maximum value of current density ($55.94 \mu\text{A cm}^{-2}$) is observed for carbon steel at a corrosion potential of -533 mV , the most cathodic one observed in Fig. 15. The current density decreases to $38.43 \mu\text{A cm}^{-2}$ for the Ni–P coatings and further decreases with increasing concentrations of TiC particles in the Ni–P matrix. Thus, the values of current density decrease to $25.62 \mu\text{A cm}^{-2}$, $7.79 \mu\text{A cm}^{-2}$, $6.49 \mu\text{A cm}^{-2}$ and $4.91 \mu\text{A cm}^{-2}$ for the 0.5 g L^{-1} , 1.0 g L^{-1} , 1.5 g L^{-1} , and 2.0 g L^{-1} TiC composite coatings respectively. Moreover, the corrosion potential, becomes slightly more anodic for the Ni–P coatings and increases from $\sim -372 \text{ mV}$ to $\sim -312 \text{ mV}$ with increasing concentrations of TiC suggesting a slight inhibition of the anodic activity in the presence of the TiC particles in the Ni–P matrix. Interestingly, for the TiC concentrations of 1.0 , 1.5 and 2.0 g L^{-1} , the anodic current density is independent of the content of TiC particles, and significantly lower compared to the Ni–P coating. This trend evidences that the anodic activity is reduced in the presence of the TiC particles (for the 3 highest concentrations). However, the cathodic current density tends to increase as the concentration of particles increases, approaching the values observed for the Ni–P coating and steel. This indicates that the cathodic processes, mainly oxygen reduction, are favored by the presence of TiC particles. The potentiodynamic polarization results show that Ni–P coatings had lower corrosion resistance compared to steel, displaying a corrosion protection efficiency of $\sim 31\%$. In such composite coatings, corrosion often initiates at grain boundaries of the nodules as result of the adsorption of chloride ions. The anodic activity leads to the formation of soluble $NiCl_2$ which can proceed to formation of pits⁷². The corrosion protection efficiency, consequence of the decreased corrosion current density, increases with the increasing concentration of TiC particles in the Ni–P matrix. The highest corrosion protection efficiency

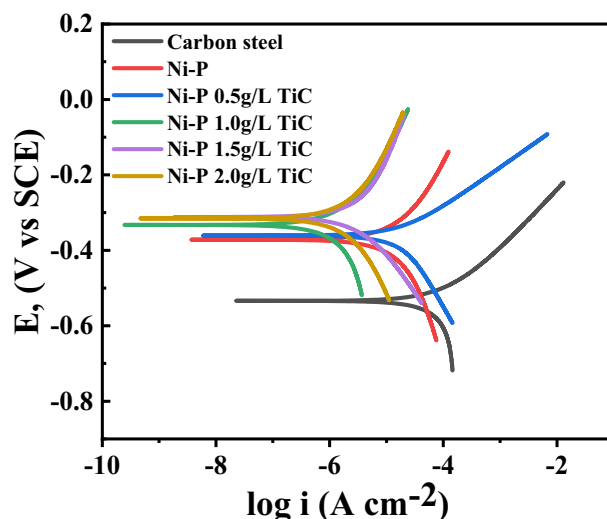


Figure 15. Potentiodynamic profiles of carbon steel, Ni-P and Ni-P-TiC composite coating with increasing concentration of TiC.

Composition	β_a (V/decade)	β_c (V/decade)	I_{corr} ($\mu A\ cm^{-2}$)	E_{corr} (mV)	PE%
Carbon steel	0.09617	0.2275	55.94	-534.0	
Ni-P	0.3514	0.6088	38.43	-372.0	31.3%
Ni-P 0.5 g L ⁻¹ TiC	0.1059	0.2664	25.62	-361.0	54.2%
Ni-P 1.0 g L ⁻¹ TiC	0.4342	0.2902	7.79	-333.0	86.0%
Ni-P 1.5 g L ⁻¹ TiC	0.4354	0.2434	6.49	-312.0	88.4%
Ni-P 2.0 g L ⁻¹ TiC	0.384	0.4246	4.91	-315.0	91.2%

Table 4. Electrochemical parameters derived from the potentiodynamic polarization curve of carbon steel, Ni-P, and Ni-P-TiC composite coating containing various concentration of TiC particles.

(~ 90%) was achieved at a TiC concentration of 2.0 g L⁻¹. To conclude, the inclusion of TiC particles in the Ni-P alloy matrix has improved the corrosion resistance as the concentration of TiC particles. By the one hand, the presence of particles inhibits the anodic reactions and, on the other hand, it contributes to reduce the number of active sites for the adsorption of chloride ions on the surface defects such as cracks and pores. Enhancement in the corrosion resistance by increased concentration of reinforcement is in good agreement with literature^{33,35,36}.

Conclusions

Ni-P-TiC composite coatings containing various concentrations of TiC particles were synthesized using the electrodeposition technique. The amount of TiC particles in the Ni-P matrix has a significant influence on its morphological, structural, mechanical, and corrosion protection properties. The hardness of Ni-P-TiC composite coatings increases with an increasing amount of TiC particles in the Ni-P matrix. However, an excessive amount of TiC particles (2.0 g L⁻¹) leads to particles agglomeration and thus reduction in hardness. Electrochemical studies confirm the increased corrosion protection offered by the Ni-P coatings with an increasing amount of TiC particles. The Ni-P-TiC composite coatings demonstrate superior mechanical and corrosion protection properties when compared to Ni-P coatings suggesting their utilization in many industries such as automobile, marine, electronic, oil, and gas industries.

Received: 12 November 2020; Accepted: 20 January 2021

Published online: 05 March 2021

References

- Zamani, S. M., Hassanzadeh-Tabrizi, S. A. & Sharifi, H. Failure analysis of drill pipe: a review. *Eng. Fail. Anal.* **59**, 605–623 (2016).
- Xie, M. & Tian, Z. A review on pipeline integrity management utilizing in-line inspection data. *Eng. Fail. Anal.* **92**, 222–239 (2018).
- Ossai, C. I., Boswell, B. & Davies, I. J. Pipeline failures in corrosive environments—a conceptual analysis of trends and effects. *Eng. Fail. Anal.* **53**, 36–58 (2015).
- Xu, X *et al.* Corrosion of stainless steel valves in a reverse osmosis system: analysis of corrosion products and metal loss. *Eng. Fail. Anal.* **105**, 40–51 (2019).
- Amaya-Gómez, R. *et al.* Reliability assessments of corroded pipelines based on internal pressure—a review. *Eng. Fail. Anal.* **98**, 190–214 (2019).

6. Bhandari, J. *et al.* Modelling of pitting corrosion in marine and offshore steel structures—a technical review. *J. Loss Prev. Process Ind.* **37**, 39–62 (2015).
7. Finšgar, M. & Jackson, J. Application of corrosion inhibitors for steels in acidic media for the oil and gas industry: a review. *Corros. Sci.* **86**, 17–41 (2014).
8. Shekari, E., Khan, F. & Ahmed, S. Economic risk analysis of pitting corrosion in process facilities. *Int. J. Press. Vessels Pip.* **157**, 51–62 (2017).
9. Shakoor, R. A. *et al.* Properties of electrodeposited Ni–B–Al₂O₃ composite coatings. *Mater. Des.* **64**, 127–135 (2014).
10. Shakoor, R. *et al.* Synthesis, characterization and applications of electroless Ni–B coatings—a review. *Int. J. Electrochem. Sci.* **11**, 2486–2512 (2016).
11. Pfeifer, M. Chapter 5 - manufacturing process considerations. In *Materials Enabled Designs* (ed. Pfeifer, M.) 115–160 (Butterworth-Heinemann, 2009).
12. Gurrappa, I. & Binder, L. Electrodeposition of nanostructured coatings and their characterization—a review. *Sci. Technol. Adv. Mater.* **9**(4), 043001 (2008).
13. Lelevic, A. & Walsh, F. C. Electrodeposition of Ni P composite coatings: a review. *Surf. Coat. Technol.* **378**, 124803 (2019).
14. Giurlani, W. *et al.* Electroplating for decorative applications: recent trends in research and development. *Coatings* **8**, 260 (2018).
15. Nava, D. *et al.* Effects of heat treatment on the tribological and corrosion properties of electrodeposited Ni–P alloys. *Int. J. Electrochem. Sci.* **8**, 2670–2681 (2013).
16. Lelevic, A. & Walsh, F. C. Electrodeposition of NiP composite coatings: a review. *Surf. Coat. Technol.* **378**, 124803 (2019).
17. Fayyad, E. *et al.* Recent advances in electroless-plated Ni–P and its composites for erosion and corrosion applications: a review. *Emerg. Mater.* **1**, 3–24 (2018).
18. Sadeghi, A. *Microstructure evolution and strengthening mechanism in Ni-based composite coatings* (2016).
19. Ma, C. *et al.* The electrodeposition and characterisation of low-friction and wear-resistant Co–Ni–P coatings. *Surf. Coat. Technol.* **235**, 495–505 (2013).
20. Bahadormanesh, B. & Ghorbani, M. Electrodeposition of Zn–Ni–P compositionally modulated multilayer coatings: an attempt to deposit Ni–P and Zn–Ni alloys from a single bath. *Electrochem. Commun.* **81**, 93–96 (2017).
21. Sknar, Y. E., Savchuk, O. O. & Sknar, I. V. Characteristics of electrodeposition of Ni and Ni–P alloys from methanesulfonate electrolytes. *Appl. Surf. Sci.* **423**, 340–348 (2017).
22. Shakoor, R. A. *et al.* Synthesis and properties of electrodeposited Ni–B–CeO₂ composite coatings. *Mater. Des.* **59**, 421–429 (2014).
23. Wang, Y. *et al.* Microstructure and properties of sol-enhanced Ni–Co–TiO₂ nano-composite coatings on mild steel. *J. Alloy. Compd.* **649**, 222–228 (2015).
24. Shakoor, R. A. *et al.* Electrodeposition of Ni–B–Zn alloy coatings and their characterization. In *Proceedings of the 4th International Gas Processing Symposium* (eds Al-Marri, M. J. & Eljack, F. T.) 149–157 (Elsevier, 2015).
25. Hansal, W. E. G. *et al.* Pulse-electrodeposited NiP–SiC composite coatings. *Electrochim. Acta* **114**, 851–858 (2013).
26. Zokis-Karathanasis, A., Milickovic-Kosanovic, T. & Deligkiozi, I. Effect of organic additives in the structure and functional properties of Ni–P composite coatings reinforced by nano-SiC and MWCNT. In *10th Pan-Hellenic Scientific Congress of Chemical Engineering, Patra* (2015).
27. Chuang, Y.-C. *et al.* Effect of surfactant on the electrodeposition of Ni–P coating in emulsified supercritical CO₂ baths. *Thin Solid Films* **529**, 322–326 (2013).
28. Alleg, S. *et al.* Microstructure and magnetic properties of NiP alloys. *J. Supercond. Nov. Magn.* **29**(4), 1001–1011 (2016).
29. Luo, H. *et al.* Synthesis of a duplex Ni–P–YSZ/Ni–P nanocomposite coating and investigation of its performance. *Surf. Coat. Technol.* **311**, 70–79 (2017).
30. Dhanapal, K., Narayanan, V. & Stephen, A. Effect of phosphorus on magnetic property of Ni–P alloy synthesized using pulsed electrodeposition. *Mater. Chem. Phys.* **166**, 153–159 (2015).
31. Elias, L., Damle, V. H. & Hegde, A. C. Electrodeposited Ni–P alloy thin films for alkaline water splitting reaction. *IOP Conf. Ser. Mater. Sci. Eng.* **149**, 012179 (2016).
32. Elias, L., Bhat, B. & Hegde, A. Development of nanolaminated multilayer Ni–P alloy coatings for better corrosion protection. *RSC Advances* **6**, 34005–34013 (2016).
33. Bahgat Radwan, A. *et al.* Properties enhancement of Ni–P electrodeposited coatings by the incorporation of nanoscale Y₂O₃ particles. *Appl. Surf. Sci.* **457**, 956–967 (2018).
34. Tamilarasan, T. R. *et al.* Wear and scratch behaviour of electroless Ni–P–nano-TiO₂: Effect of surfactants. *Wear* **346–347**, 148–157 (2016).
35. Farzaneh, A. *et al.* Electrochemical and structural properties of electroless Ni–P–SiC nanocomposite coatings. *Appl. Surf. Sci.* **276**, 697–704 (2013).
36. Sadreddini, S. & Afshar, A. Corrosion resistance enhancement of Ni–P–nano SiO₂ composite coatings on aluminum. *Appl. Surf. Sci.* **303**, 125–130 (2014).
37. Jin, H., Jiang, S. & Zhang, L. Structural characterization and corrosive property of Ni–P/CeO₂ composite coating. *J. Rare Earths* **27**(1), 109–113 (2009).
38. Li, C. *et al.* Microstructure evolution and mechanical properties of reactive plasma sprayed Ti₃SiC₂–Ti₅Si₃–TiC composite coatings. *Mater. Chem. Phys.* **254**, 123495 (2020).
39. He, X., Song, R. G. & Kong, D. J. Effects of TiC on the microstructure and properties of TiC/TiAl composite coating prepared by laser cladding. *Opt. Laser Technol.* **112**, 339–348 (2019).
40. Wang, C. *et al.* Indentation and bending behavior of electroless Ni–P–Ti composite coatings on pipeline steel. *Surf. Coat. Technol.* **334**, 243–252 (2018).
41. Balaraju, J. N., Sankara Narayanan, T. S. N. & Seshadri, S. K. Electroless Ni–P composite coatings. *J. Appl. Electrochem.* **33**(9), 807–816 (2003).
42. Radwan, A. B. & Shakoor, R. A. Aluminum nitride (AlN) reinforced electrodeposited Ni–B nanocomposite coatings. *Ceram. Int.* **46**(7), 9863–9871 (2020).
43. Yusuf, M. *et al.* Synthesis and characterisation of Ni–B/Ni–P–CeO₂ duplex composite coatings. *J. Appl. Electrochem.* **48**, 391–404 (2018).
44. Yang, Y. *et al.* Fabrication and characterization of electroless Ni–P–ZrO₂ nano-composite coatings. *Appl. Nanosci.* **1**(1), 19–26 (2011).
45. Knyazev, A. V. *et al.* Magnetic properties of electrodeposited amorphous nickel–phosphorus alloys. *Russ. J. Electrochem.* **53**(3), 270–274 (2017).
46. Afroukhteh, S., Dehghanian, C. & Emamy, M. Preparation of electroless Ni–P composite coatings containing nano-scattered alumina in presence of polymeric surfactant. *Prog. Nat. Sci. Mater. Int.* **22**, 318–325 (2012).
47. Li, B. & Zhang, W. Microstructural, surface and electrochemical properties of pulse electrodeposited Ni–W/Si₃N₄ nanocomposite coating. *Ceram. Int.* **44**(16), 19907–19918 (2018).
48. Safavi, M. S. & Rasooli, A. Ni–P–TiO₂ nanocomposite coatings with uniformly dispersed Ni₃Ti intermetallics: effects of current density and post heat treatment. *Surf. Coat. Technol.* **372**, 252–259 (2019).
49. Sliem, M. H. *et al.* Enhanced mechanical and corrosion protection properties of pulse electrodeposited NiP–ZrO₂ nanocomposite coatings. *Surf. Coat. Technol.* **403**, 126340 (2020).

50. Restrepo Parra, E., Arango, P. J. & Benavides, V. XPS structure analysis of TiN/TiC bilayers produced by pulsed vacuum arc discharge. *Dyna* **77**, 64–74 (2010).
51. Spanou, S. *et al.* Self cleaning behaviour of Ni/nano-TiO₂ metal matrix composites. *Electrochim. Acta* **105**, 324–332 (2013).
52. Pillai, A. M., Rajendra, A. & Sharma, A. K. Electrodeposited nickel–phosphorous (Ni–P) alloy coating: an in-depth study of its preparation, properties, and structural transitions. *J. Coat. Technol. Res.* **9**(6), 785–797 (2012).
53. Ping, Z. *et al.* Mechanically assisted electroplating of Ni–P coatings on carbon steel. *Surf. Coat. Technol.* **202**(24), 6023–6028 (2008).
54. Guglielmi, N. Kinetics of the deposition of inert particles from electrolytic baths. *J. Electrochem. Soc.* **119**(8), 1009 (1972).
55. Berçot, P., Peña-Muñoz, E. & Pagetti, J. Electrolytic composite Ni–PTFE coatings: an adaptation of Guglielmi's model for the phenomena of incorporation. *Surf. Coat. Technol.* **157**(2), 282–289 (2002).
56. Bahadormanesh, B. & Dolati, A. The kinetics of Ni–Co/SiC composite coatings electrodeposition. *J. Alloy. Compd.* **504**(2), 514–518 (2010).
57. Fransaer, J., Celis, J. P. & Roos, J. R. Analysis of the electrolytic codeposition of non-Brownian particles with metals. *J. Electrochem. Soc.* **139**(2), 413–425 (1992).
58. Celis, J. P., Roos, J. R. & Buelens, C. A mathematical model for the electrolytic codeposition of particles with a metallic matrix. *J. Electrochem. Soc.* **134**(6), 1402–1408 (1987).
59. Pouladi, S., Shariat, M. H. & Bahrololoom, M. E. Electrodeposition and characterization of Ni–Zn–P and Ni–Zn–P/nano-SiC coatings. *Surf. Coat. Technol.* **213**, 33–40 (2012).
60. Huang, H.-C. *et al.* Microstructure evolution and hardening mechanisms of Ni–P electrodeposits. *Surf. Coat. Technol.* **205**(7), 2097–2103 (2010).
61. Balaraju, J. N., Narayanan, T. S. N. S. & Seshadri, S. K. Structure and phase transformation behaviour of electroless Ni–P composite coatings. *Mater. Res. Bull.* **41**(4), 847–860 (2006).
62. Grove, D. E., Gupta, U. & Castleman, A. W. Effect of carbon concentration on changing the morphology of titanium carbide nanoparticles from cubic to cuboctahedron. *ACS Nano* **4**(1), 49–54 (2010).
63. Zhou, Y.-R. *et al.* Electrodeposition and corrosion resistance of Ni–P–TiN composite coating on AZ91D magnesium alloy. *Trans. Nonferrous Met. Soc. China* **26**(11), 2976–2987 (2016).
64. Wang, Y. *et al.* Duplex Ni–P–ZrO₂/Ni–P electroless coating on stainless steel. *J. Alloy. Compd.* **630**, 189–194 (2015).
65. Yusuf, M. M. *et al.* Synthesis and characterisation of Ni–B/Ni–P–CeO₂ duplex composite coatings. *J. Appl. Electrochem.* **48**(4), 391–404 (2018).
66. Meshram, A. P., Punith Kumar, M. K. & Srivastava, C. Enhancement in the corrosion resistance behaviour of amorphous NiP coatings by incorporation of graphene. *Diamond Relat. Mater.* **105**, 107795 (2020).
67. Ghavidel, N. *et al.* Corrosion and wear behavior of an electroless Ni–P/nano-SiC coating on AZ31 Mg alloy obtained through environmentally-friendly conversion coating. *Surf. Coat. Technol.* **382**, 125156 (2020).
68. Czagány, M. & Baumli, P. Effect of surfactants on the behavior of the Ni–P bath and on the formation of electroless Ni–P–TiC composite coatings. *Surf. Coat. Technol.* **361**, 42–49 (2019).
69. Fayyad, E. M. *et al.* Novel electroless deposited corrosion-resistant and anti-bacterial NiP–TiNi nanocomposite coatings. *Surf. Coat. Technol.* **369**, 323–333 (2019).
70. Luo, H. *et al.* Development of electroless Ni–P/nano-WC composite coatings and investigation on its properties. *Surf. Coat. Technol.* **277**, 99–106 (2015).
71. Luo, H. *et al.* Characterization of microstructure and properties of electroless duplex Ni–W–P/Ni–P nano-ZrO₂ composite coating. *Mater. Today Phys.* **4**, 36–42 (2018).
72. Song, Y., Shan, D. & Han, E. Comparative study on corrosion protection properties of electroless NiP–ZrO₂ and NiP coatings on AZ91D magnesium alloy. *Mater. Corros. werkstoffe Und Korrosion - MATER CORROS* **58**, 506–510 (2007).

Acknowledgments

This publication was made possible by Qatar University Grant-IRCC-2020-006. Statements made herein are solely the responsibility of the authors. Microstructural analyses (FE-SEM/EDS and HR-TEM) were accomplished at the Central Laboratory Unit (CLU), Qatar University, Doha, Qatar. XPS analysis was accomplished at the Gas Processing Center (GPC), Qatar University, Doha, Qatar. Prof. M. F. Montemor thanks Fundação para a Ciência e a Tecnologia (FCT, Portugal) for financial support under the projects UIDB/00100/2020.

Author contributions

O.F. developed coatings and wrote the initial draft of the manuscript, Adnan Khan helped in experimental work and corrosion studies, R.A.S. designed the experiments and revised the manuscript, A.H. helped in the analysis of mechanical properties of the coatings, M.M.Y. conducted the mechanical testing, M.F.M. revised and corrected the corrosion part and entire manuscript, S.R. modified and revised the whole manuscript, K.K. helped in the analyzing the microstructures of the coatings and revised that part of the manuscript, M.R.I.F. helped in XPS analysis and P.C.O. revised and modified the whole manuscript.

Competing interests

The authors declare no competing interests.

Additional information

Correspondence and requests for materials should be addressed to R.A.S.

Reprints and permissions information is available at www.nature.com/reprints.

Publisher's note Springer Nature remains neutral with regard to jurisdictional claims in published maps and institutional affiliations.



Open Access This article is licensed under a Creative Commons Attribution 4.0 International License, which permits use, sharing, adaptation, distribution and reproduction in any medium or format, as long as you give appropriate credit to the original author(s) and the source, provide a link to the Creative Commons licence, and indicate if changes were made. The images or other third party material in this article are included in the article's Creative Commons licence, unless indicated otherwise in a credit line to the material. If material is not included in the article's Creative Commons licence and your intended use is not permitted by statutory regulation or exceeds the permitted use, you will need to obtain permission directly from the copyright holder. To view a copy of this licence, visit <http://creativecommons.org/licenses/by/4.0/>.

© The Author(s) 2021